

Thermophysical properties of warm dense hydrogen

Bastian Holst and Ronald Redmer

Universität Rostock, Institut für Physik, D-18051 Rostock, Germany

Michael P. Desjarlais

Pulsed Power Sciences Center, Sandia National Laboratories, Albuquerque, New Mexico 87185-1186, USA

(Dated: October 22, 2018)

We study the thermophysical properties of warm dense hydrogen using quantum molecular dynamics simulations. New results are presented for the pair distribution functions, the equation of state, the Hugoniot curve, and the reflectivity. We compare with available experimental data and predictions of the chemical picture. Especially, we discuss the nonmetal-to-metal transition which occurs at about 40 GPa in the dense fluid.

PACS numbers: 31.15.Ar, 61.20.Ja, 62.50.+p, 64.30.+t, 72.20.-i, 71.30.+h

I. INTRODUCTION

Hydrogen is an essential element for models of stellar and planetary interiors^{1,2}. The isotopes deuterium and tritium are considered as target materials (D-T gas) in inertial confinement fusion experiments³. Therefore, numerous efforts have been made both experimentally and theoretically to understand the behavior of hydrogen, deuterium, and tritium in a wide range of densities and temperatures. In particular, progress in shock-wave experimental technique has allowed the systematic probing of the megabar pressure range, so that a sound database has been assembled within the last decade. Single or multiple shock-wave experiments have been performed for hydrogen (or deuterium) by using, e.g., high explosives⁴, gas guns⁵, pulsed power^{6,7,8}, or high-power lasers⁹. The combination of high pressures and temperatures of several eV defines *warm dense matter*, a strongly correlated state relevant for planetary interiors which is characterized by partial ionization where the bound states exhibit a highly transient nature.

Furthermore, the enormous progress in computer capacity has allowed the development and application of *ab initio* simulation techniques for warm dense matter such as Path Integral Monte Carlo (PIMC)¹⁰ or Quantum Molecular Dynamics (QMD) simulations¹¹ which treat quantum effects and correlations systematically. These techniques give already highly predictive results for a variety of problems and systems; see Ref. 12 for QMD simulations.

The equation of state (EOS) and derived quantities such as the Hugoniot curve, the sound velocity, or the Grüneisen parameter are important material properties in this context. Furthermore, optical properties as, e.g., the reflectivity are closely related to the dielectric function which also determines the dc electrical conductivity in the static limit. All these quantities are used to characterize the unique behavior of warm dense hydrogen, especially for high pressures at, or exceeding, one megabar,

where a transition from a nonconducting, molecular fluid to a mono-atomic fluid with metallic-like conductivity occurs. Describing the disordered fluid in terms of solid state parameters, the fundamental band gap between the valence and conduction band decreases with the pressure and, subsequently, the electrical conductivity shows an exponential increase as is typical for thermally activated transport in semiconductors¹³. For pressures above 1.4 Mbar, conductivities of about $2000 \Omega^{-1} \text{ cm}^{-1}$, as is characteristic for simple metallic fluids such as Cs, have been observed experimentally around $3000 \text{ K}^{14,15}$, and band gap closure has been claimed to be responsible for this nonmetal-to-metal transition.

On the other hand, concepts of plasma physics have been applied to warm dense matter states¹⁶. For instance, the chemical picture gives a rather simple description by identifying stable bound states out of elementary particles as new composite particles. Hydrogen at normal conditions in this context is a molecular fluid. Free electrons are generated at high pressure by dissociation of molecules, $\text{H}_2 \rightleftharpoons 2 \text{H}$, and a subsequent ionization of atoms, $\text{H} \rightleftharpoons \text{e} + \text{p}$. This model yields already the strong increase of the conductivity with the pressure (pressure ionization). In addition, bound states contribute to conduction via hopping processes¹⁷. The conceptual problem of all chemical models is the clear definition of bound states, the derivation of effective potentials between all species, and the calculation of cross sections for the respective scattering processes in a strongly correlated medium.

QMD simulations are a powerful tool to describe warm dense matter^{18,19,20,21,22}. The combination of classical molecular dynamics for the ions and density functional theory (DFT) for the electrons allows one to consider correlation and quantum effects. Alternatively, wave packet simulations have been developed in which the electrons are represented on a semi-quantal level by wave packets (WPMD)^{23,24,25,26,27,28}.

In this paper, we apply QMD simulations and calculate

a broad spectrum of thermophysical properties of warm dense hydrogen. We determine EOS data for a wide region of densities and temperatures and compare with chemical models. We calculate the principal Hugoniot curve for liquid targets. The Kubo-Greenwood formula serves as a starting point for the evaluation of the dynamic conductivity $\sigma(\omega)$ from which the dielectric function $\varepsilon(\omega)$ and the reflectivity can be extracted. In addition, the electronic structure calculation within DFT yields the charge density distribution in the simulation box at every time step, and the molecular dynamics run gives valuable structural information via the ion-ion pair correlation function. This is important for the identification and characterization of phase transitions such as solid-liquid or liquid-plasma as well as for the nonmetal-to-metal transition.

II. QMD SIMULATIONS

Within QMD simulations we perform molecular dynamics simulations with a quantum mechanical treatment of the electrons by using density functional theory (DFT). This is based upon the theorems of Hohenberg and Kohn²⁹ and gives the electron density that minimizes the ground state energy of the system. It has been proven that this density is a unique functional of the effective potential V_{eff} .

From this formalism Kohn and Sham³⁰ derived a computational scheme which solves the problem for a fictitious system of non-interacting particles that leads to the same electron density. This scheme consists basically of solving the Kohn-Sham equations

$$\left[-\frac{\hbar^2}{2m}\nabla^2 + V_{\text{eff}}(r)\right]\varphi_k(r) = \epsilon_k\varphi_k(r), \quad (1)$$

$$V_{\text{eff}}[\varrho(\mathbf{r})] = \int \frac{\varrho(\mathbf{r}')e^2}{|\mathbf{r}-\mathbf{r}'|} d\mathbf{r}' - \sum_{k=1}^N \frac{Z_k e^2}{|\mathbf{r}-\mathbf{R}_k|} + V_{XC}[\varrho(\mathbf{r})].$$

Our *ab initio* quantum molecular dynamics simulations were performed within Mermin's finite temperature density functional theory (FT-DFT)³¹, which is implemented in the plane wave density functional code VASP (Vienna Ab Initio Simulation Package)^{32,33,34}. We used the projector augmented wave potentials³⁵ and did a generalized gradient approximation (GGA) using the parameterization of PBE³⁶. Extensive test calculations, as performed already by Desjarlais²², have shown that the EOS data are dependent on the plane wave cutoff. A convergence of better than 1% is secured for $E_{\text{cut}} = 1200$ eV which was used in all actual calculations. The electronic structure calculations were performed for a given array of ion positions which are subsequently varied by the forces obtained within the DFT calculations via the Hellmann-Feynman theorem for each molecular dynamics step. This schema is repeated until the EOS measures are converged and a thermodynamic equilibrium is reached.

The simulations were done for 64 atoms in a supercell with periodic boundary conditions. The temperature of the ions was controlled by a Nosé thermostat³⁷ and the temperature of the electrons was fixed by Fermi weighting the occupation of bands³³. The Brillouin zone was sampled by evaluating the results at Baldereschi's mean value point³⁸ which showed best agreement with a sampling of the Brillouin zone using a higher number of \mathbf{k} -points. The density of the system was fixed by the size of the simulated supercell. To achieve a small statistical error due to fluctuations the system was simulated 1000-1500 steps further after reaching the thermodynamic equilibrium. The EOS data and pair correlation functions were then obtained by averaging over all particles and simulation steps in equilibrium. Similar calculations were performed recently for the thermophysical properties of warm dense helium³⁹ in order to verify the nonmetal-to-metal transition at high pressures.

The zero-point vibrational energy of the H₂ molecules is not included in DFT calculations. In previous calculations, the energy $\frac{1}{2}h\nu_{\text{vib}}$ per molecule is simply added which is very important, especially at low temperatures and for the calculation of an exact initial internal energy for the reference state of the Hugoniot curve, which is 0.0855 g/cm³ at 20 K. To account for this quantum effect more sensitively for arbitrary temperatures, the fraction of molecules has to be derived, e.g., for all states along the Hugoniot curve. This can be done via the coordination number

$$K(r) = \frac{N-1}{V} \int_0^r 4\pi r'^2 g(r') dr', \quad (2)$$

which is a weighted integral over the pair correlation function $g(r)$ of the ions. N denotes the number of ions and V the volume of the supercell in the simulation. The doubled value of K at the maximum of the molecular peak in $g(r)$, which is found around $r = 0.748$ Å, is then equal to the fraction of ions bound to a molecule and twice the amount of molecules in the supercell. An example is shown in Fig. 1 where the increasing dissociation with higher density can be seen. In Fig. 2 we show the thermal dissociation; the molecular peak disappears with increasing temperature at constant density. Note that the peak is thermally broadened.

The dissociation degree is calculated for a number of isotherms and then approximated by a Fermi function which has two adjustable parameters. These parameters can be represented by temperature-dependent functions so that the dissociation degree and, subsequently, the contribution of molecules to the zero-point internal energy are determined for arbitrary temperatures. The results show that molecules can be neglected above 10,000 K.

We compare the resulting dissociation degree with that derived by Vorberger *et al.*⁴⁰ in Fig. 3. They counted all pairs of atoms in a range of 1.8 a_B as atoms. In a second step they reduced the number of molecules by counting only those pairs that are stable for longer than ten vibra-

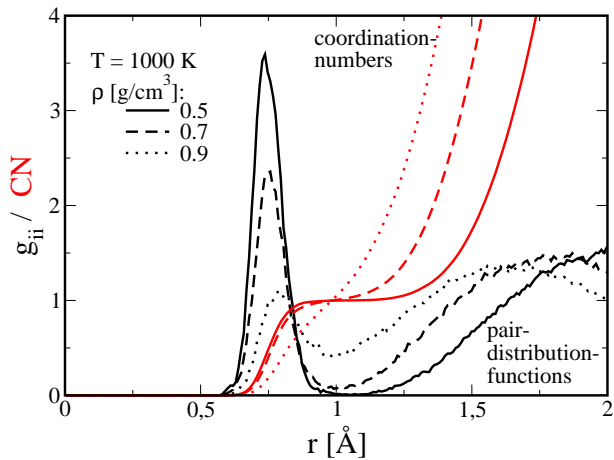


FIG. 1: Proton-proton pair distribution function and corresponding coordination numbers according to Eq. (2) for 1000 K and three densities.

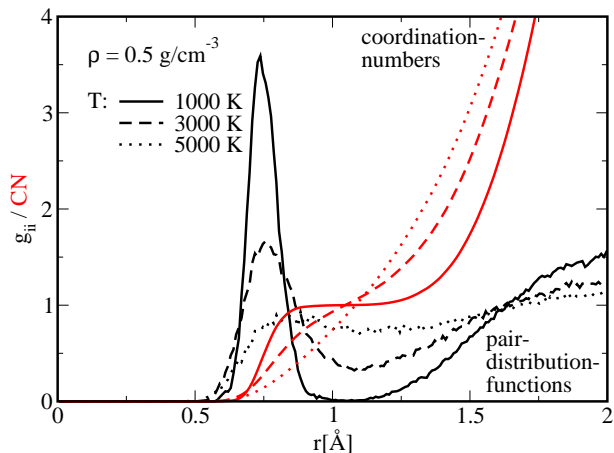


FIG. 2: Proton-proton pair distribution function and corresponding coordination numbers according to Eq. (2) for 0.5 g/cm^3 and three temperatures.

tional periods. In all three cases the amount of molecules is lower for higher densities and the molecules disappear at higher temperatures due to thermal dissociation. This picture shows that the dissociation degree depends strongly on the definition of the term *molecule* in the warm dense matter region. Our alternative method gives a smoother behavior of the dissociation degree which starts at lower temperatures and is in between the two cases described by Vorberger *et al.*⁴⁰ at higher temperatures.

III. RESULTS FOR THE EOS AND HUGONIOT CURVES

We show the thermal EOS of warm dense hydrogen in Fig. 4. The isotherms of the pressure show a systematic behavior in terms of the density and temperature. We

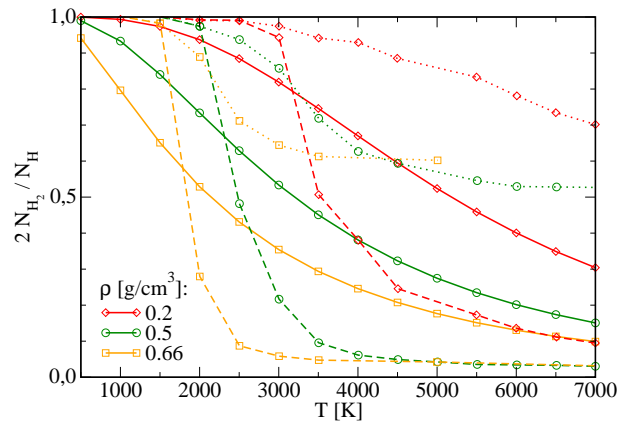


FIG. 3: Ratio of hydrogen molecules with respect to the total number of protons for three densities: Our coordination number method (solid) is compared with the pair-counting method of Vorberger *et al.*⁴⁰ (dotted). Their result counting only pairs with a lifetime longer than ten H_2 vibrational periods is also given (dashed line).

find no indication of a plasma phase transition (PPT) which would result in an instability of the EOS isotherms that would need to be treated by a Maxwell construction⁴¹. The absence of a PPT is in contrast to results of chemical models which use, e.g., Fluid Variational Theory (FVT)^{42,43,44} or liquid state perturbation theory⁴⁵. Chemical models are based on a free energy minimization schema for a mixture of hydrogen atoms, molecules, and a plasma in chemical equilibrium. Correlations are taken into account based on effective two-particle potentials. The description of the free charged particles (plasma) is done beyond the Debye-Hückel approximation by using efficient Padé formulas which are valid for a wide region of densities and temperatures.

In Fig. 4 our QMD results are compared with the chemical models FVT⁴⁴ and SCvH-i⁴⁵. The EOS derived by Saumon *et al.*⁴⁵ shows also a PPT (SCvH-ppt data set). The modified SCvH-i data set shown here avoids the PPT by using an interpolation through the instability region. Therefore, both data sets can be used to study the influence of a PPT on interior models of giant planets such as Jupiter. Consistent chemical models yield the correct low-temperature and low-density limit and agree with our QMD results there. A good agreement is also found in the high-density limit where a nearly temperature independent behavior characteristic of a degenerate plasma is found. At medium densities the pressure isotherms of FVT and SCvH-i lie well below the QMD data; the deviations amount up to 25%.

We have encountered a region with $(\partial P / \partial T)_V < 0$, which was previously reported by Vorberger *et al.*⁴⁰. It can be related to the rapid dissociation transition at low temperatures.

Following Lenosky *et al.*⁴⁶ and Beule *et al.*⁴⁷ we fit smooth functions for the pressure P and the internal energy U as an expansion in terms of density ρ and tem-

TABLE I: Coefficients a_{ik} in the expansion for the pressure P^{int} according to Eqs. (4) and (5).

i	a_{i0}	a_{i1}	a_{i2}	a_{i3}	a_{i4}
0	0.2234	2919.84	3546.67	1.94023	$1.11316 \cdot 10^{-6}$
1	14.7586	2117.98	4559.17	-17.9538	$4.88041 \cdot 10^{-4}$
2	-33.8469	2693.63	4159.13	70.582	$-2.8848 \cdot 10^{-4}$

TABLE II: Coefficients b_{jk} in the expansion for the specific internal energy u according to Eqs. (6) and (7).

j	b_{j0}	b_{j1}	b_{j2}	b_{j3}	b_{j4}
0	-33.8377	2154.38	3696.89	-300.446	$1.77956 \cdot 10^{-2}$
1	55.8794	3174.39	2571.21	56.222	$-3.56234 \cdot 10^{-3}$
2	-30.0376	3174.02	2794.39	87.3659	$2.0819 \cdot 10^{-3}$
3	5.57328	3215.51	2377.23	-13.1622	$-3.84004 \cdot 10^{-4}$
4	-0.3236	3245.48	2991.45	0.682152	$2.19862 \cdot 10^{-5}$

perature T to the given results of the QMD simulations. The pressure is split into an ideal and an interaction contribution:

$$P = P^{id} + P^{int} = \frac{\rho k_B T}{m_H} + P^{int}(\rho, T). \quad (3)$$

The QMD data for the pressure P given in kbar can be interpolated by the following expansion for the interaction contribution:

$$P^{int}(\rho, T) = (A_1(T) + A_2(T)\rho)^{A_0(T)}, \quad (4)$$

$$A_i(T) = a_{i0} \exp\left(-\left(\frac{T - a_{i1}}{a_{i2}}\right)^2\right) + a_{i3} + a_{i4}T. \quad (5)$$

The coefficients a_{ik} are summarized in Tab. I.

The QMD data for the specific internal energy $u = U/m$ given in kJ/g can be interpolated by a similar expansion:

$$u = \sum_{j=0}^4 B_j(T)\rho^j, \quad (6)$$

$$B_j(T) = b_{j0} \exp\left(-\left(\frac{T - b_{j1}}{b_{j2}}\right)^2\right) + b_{j3} + b_{j4}T. \quad (7)$$

The expansion coefficients b_{jk} are given in Tab. II.

The expansions (4) and (6) reproduce the *ab initio* QMD data within 5% accuracy in a density range from 0.5 g/cm^3 to 5 g/cm^3 between 500 K and 20000 K and can easily be applied in planetary models or hydrodynamic simulations for warm dense matter. The expansions fulfill thermodynamic consistency expressed by the relation

$$P - T \left(\frac{\partial P}{\partial T}\right)_V = - \left(\frac{\partial U}{\partial V}\right)_T \quad (8)$$

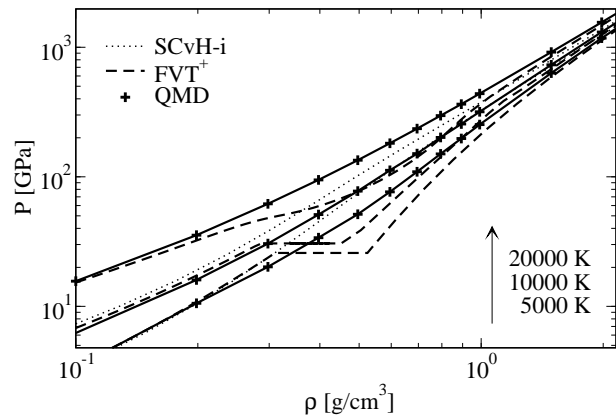


FIG. 4: Thermal EOS for warm dense hydrogen (pressure isotherms): QMD data are compared with the chemical models FVT⁺⁴⁴ and SCvH-i⁴⁵.

within 15% accuracy which is mainly due to the deviations from the QMD data itself.

A crucial measure for theoretical EOS data is the principal Hugoniot curve which is plotted in Fig. 5. It describes all possible final states (ρ, P, u) of shock wave experiments according to the Hugoniot equation

$$u - u_0 = \frac{1}{2}(P + P_0)\left(\frac{1}{\rho_0} - \frac{1}{\rho}\right) \quad (9)$$

starting at the same initial conditions (ρ_0, P_0, u_0) . For the hydrogen principal Hugoniot curve, the initial density is $\rho_0 = 0.0855 \text{ g/cm}^3$ and the initial internal energy $u_0 = -314 \text{ kJ/g}$ at a temperature of 20 K. The initial pressure P_0 can be neglected because of the high pressure of the final state.

Shock wave experiments have been performed for deuterium using gas guns⁴⁸, magnetically launched flyer plates at Sandia's Z machine⁸ or high explosives (HE)⁴⁹. These experiments indicate a maximum compression of 4.25 at about 50 GPa.

Another series of laser-driven experiments⁹ shows systematic deviations from the experiments quoted above. Especially, a maximum compression of 6 has been reported at about 1 Mbar. According to the unanimous evaluation of the shock-wave experimental data for molecular liquids⁵, we compare our QMD data in Fig. 5 only with the data sets mentioned above.

The systematic increase of the cutoff energy E_{cut} in QMD simulations from 500 eV⁵⁰ to 1200 eV²² has led to fully converged results in agreement with the experimental points. The consideration of the zero-point vibrations of the H_2 molecules along the entire Hugoniot curve yields a very good agreement of QMD data with the gas gun experiments⁴⁸ especially for low pressures. The calculated Hugoniot curve has a maximum compression of 4.5 which is slightly higher than the HE and Z experiments indicate (about 4.25). This is an agreement of about 5% accuracy which can be translated into an accuracy of about 1% in the measured shock and particle

velocity, which is in the range of the systematic errors in the experiments. The compression decreases with higher pressures and temperatures and reaches the correct high-temperature limit as given by the PIMC simulations⁵¹. The QMD curve lies slightly below the experimental data for compression rates between 3 and 4 which could be due to the known band gap problem of DFT in GGA. The FVT curve⁴² is shown as a representative of chemical models which, in general, show a higher compressibility well beyond 4.5.

Also shown is the linear mixing result of Ross⁵². This curve shows a sixfold compression and is not in agreement with the shown experiments. The curve of Kerley⁵³ has a maximum compression of 4.25, like the experiments indicate, but the pressure is there slightly higher than the results of the QMD simulations.

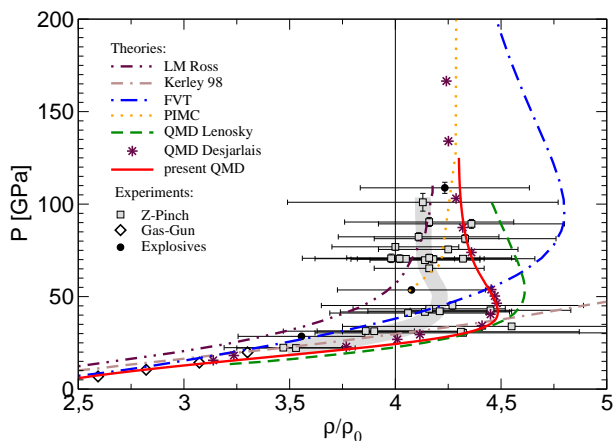


FIG. 5: Principal Hugoniot curve for hydrogen. The results of this work (solid line) are compared with previous QMD results of Lenosky *et al.*⁵⁰ (dashed) and Desjarlais²² (stars), PIMC simulations⁵⁴ (dotted), the linear mixing model of Ross⁵² (dot-dash-dashed), the model of Kerley⁵³ (dot-dot-dashed) and the chemical model FVT⁴² (dashed). Experiments: Gas gun⁴⁸ (diamonds), Sandia Z machine⁸ (grey squares; grey line: running average through the u_s - u_p data), high explosives⁴⁹ (black circles).

IV. DYNAMIC CONDUCTIVITY, REFLECTIVITY AND DC CONDUCTIVITY

The dynamic conductivity $\sigma(\omega)$ is derived from the Kubo-Greenwood formula:^{55,56}

$$\sigma(\omega) = \frac{2\pi e^2 \hbar^2}{3m^2 \omega \Omega} \sum_{\mathbf{k}} W(\mathbf{k}) \sum_{j=1}^N \sum_{i=1}^N \sum_{\alpha=1}^3 [F(\epsilon_{i,\mathbf{k}}) - F(\epsilon_{j,\mathbf{k}})] \times |\langle \Psi_{j,\mathbf{k}} | \nabla_{\alpha} | \Psi_{i,\mathbf{k}} \rangle|^2 \delta(\epsilon_{j,\mathbf{k}} - \epsilon_{i,\mathbf{k}} - \hbar\omega), \quad (10)$$

where e is the electron charge and m its mass. The summations over i and j run over N discrete bands considered in the electronic structure calculation for the cubic supercell volume Ω . The three spatial directions are averaged by the α sum. $F(\epsilon_{i,\mathbf{k}})$ describes the occupation

of the i th band corresponding to the energy $\epsilon_{i,\mathbf{k}}$ and the wavefunction $\Psi_{i,\mathbf{k}}$ at \mathbf{k} . The δ -function has to be broadened because a discrete energy spectrum results from the finite simulation volume²¹. Integration over the Brillouin zone is performed by sampling special \mathbf{k} points⁵⁷, where $W(\mathbf{k})$ is the respective weighting factor. We used Baldereschi's mean value point³⁸ to reach a convergence of better than 10% accuracy.

Optical properties can be derived from the frequency-dependent conductivity Eq. (10). The standard method is to obtain the imaginary part via the Kramers-Kronig relation

$$\sigma_2(\omega) = -\frac{2}{\pi} \text{P} \int \frac{\sigma_1(\nu)\omega}{(\nu^2 - \omega^2)} d\nu, \quad (11)$$

P is the principal value of the integral. The dielectric function can be calculated directly with the conductivity:

$$\epsilon_1(\omega) = 1 - \frac{1}{\epsilon_0 \omega} \sigma_2(\omega), \quad (12)$$

$$\epsilon_2(\omega) = \frac{1}{\epsilon_0 \omega} \sigma_1(\omega). \quad (13)$$

The square of the index of refraction contains the real part n and the imaginary part k is equal to the dielectric function which leads to the following relations:

$$n(\omega) = \frac{1}{2} \sqrt{|\epsilon(\omega)| + |\epsilon_1(\omega)|}, \quad (14)$$

$$k(\omega) = \frac{1}{2} \sqrt{|\epsilon(\omega)| - |\epsilon_1(\omega)|}. \quad (15)$$

The index of refraction is then used to calculate optical properties such as the reflectivity r :

$$r(\omega) = \frac{[1 - n(\omega)]^2 + k(\omega)^2}{[1 + n(\omega)]^2 + k(\omega)^2}. \quad (16)$$

We compare our *ab initio* results with reflectivities measured along the Hugoniot curve⁵⁸ in Fig. 6; the agreement is excellent. The change of the hydrogen reflectivity with the pressure can be interpreted as a gradual transition from a molecular insulating fluid through an atomic fluid above 20 GPa where the atoms have strongly fluctuating bonds with next neighbors²⁰ to a dense, almost fully ionized plasma with a reflectivity of about 50-60 % at high pressures above 40 GPa. The chemical model⁵⁹ shows also this qualitative behavior but the abrupt increase of the reflectivity occurs at a higher density. This shows the difficulties of the chemical models in finding the correct shifts of the dissociation and ionization energies as function of density and temperature and, thus, the location of the nonmetal-to-metal transition. However, the limits of a molecular fluid at low pressures and of a fully ionized plasma at high pressures are incorporated in a reasonable way.

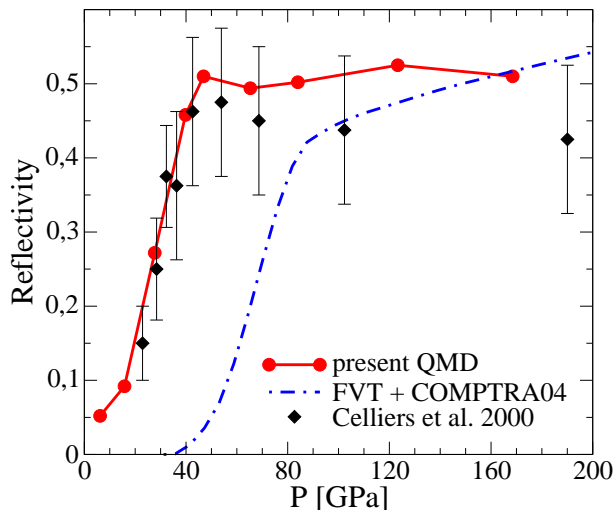


FIG. 6: Reflectivity for a wavelength of 808 nm along the Hugoniot curve of hydrogen: QMD results are compared with experimental data of Celliers *et al.*⁵⁸ and predictions of the chemical model FVT⁵⁹ using the COMPTRA code⁶⁰.

V. CONCLUSION

We have performed *ab initio* QMD simulations to study thermophysical properties of hydrogen under extreme conditions. As a result we obtained highly converged EOS data which are relevant for modeling giant planets and for the understanding of the fundamental behavior of hydrogen at high pressure. The deviations between our QMD data and chemical models amount up to 25%. We have constructed smooth fit functions for the QMD data for the pressure and the internal energy which

can be used easily in, e.g., hydrodynamic simulations for warm dense hydrogen and in astrophysical applications.

The results show a smooth transition from a molecular liquid to an atomic fluid of metal-like state. There were no signs of a PPT which is predicted by other models.

With these EOS results we have calculated the principal Hugoniot curve which is in agreement with dynamic experiments and has the correct high-temperature limit as given by PIMC simulations.

We obtained optical properties using the Kubo-Greenwood formula. The reflectivity along the Hugoniot curve is in excellent agreement with experiments. The results show the occurrence of a nonmetal-to-metal transition at about 40 GPa.

Acknowledgments

We thank P.M. Celliers, W. Ebeling, V.E. Fortov, M. French, A. Höll, A. Kietzmann, W.D. Kraeft, T.R. Mattsson, B. Militzer, V.B. Mintsev, N. Nettelmann, H. Reinholz, G. Röpke, N.A. Tahir, V.Ya. Ter-novoi, C. Toepffer, and G. Zwicknagel for stimulating discussions and for providing us with their data. This work was supported by the Deutsche Forschungsgemeinschaft within the SFB 652 and the grant mvp00006 of the High Performance Computing Center North (HLRN). We acknowledge support of the computer center of the University of Rostock (URZ). Sandia is a multiprogram laboratory operated by Sandia Corporation, a Lockheed Martin Company, for the United States Department of Energy's National Nuclear Security Administration under contract DE-AC04-94AL85000.

-
- ¹ T. Guillot, *Science* **286**, 72 (1999).
 - ² T. Guillot, *Planet. Space Sci.* **47**, 1183 (1999).
 - ³ J. D. Lindl, P. Amendt, R. L. Berger, S. G. Glendinning, S. H. Glenzer, S. W. Haan, R. L. Kauffman, O. L. Landen, and L. J. Suter, *Phys. Plasmas* **11**, 339 (2004).
 - ⁴ V. B. Mintsev and V. E. Fortov, *J. Phys. A: Math. Gen.* **39**, 4319 (2006).
 - ⁵ W. J. Nellis, *Rep. Prog. Phys.* **69**, 1479 (2006).
 - ⁶ M. D. Knudson, D. L. Hanson, J. E. Bailey, C. A. Hall, J. R. Asay, and W. W. Anderson, *Phys. Rev. Lett.* **87**, 225501 (2001).
 - ⁷ M. D. Knudson, D. L. Hanson, J. E. Bailey, C. A. Hall, and J. R. Asay, *Phys. Rev. Lett.* **90**, 035505 (2003).
 - ⁸ M. D. Knudson, D. L. Hanson, J. E. Bailey, C. A. Hall, J. R. Asay, and C. Deeney, *Phys. Rev. B* **69**, 144209 (2004).
 - ⁹ R. Cauble, L. B. D. Silva, T. S. Perry, D. R. Bach, K. S. Budil, P. Celliers, G. W. Collins, A. Ng, T. W. Barbee Jr., B. A. Hammel, et al., *Phys. Plasmas* **4**, 1857 (1997).
 - ¹⁰ D. M. Ceperley and E. Manousakis, *J. Chem. Phys.* **115**, 10111 (2001).
 - ¹¹ L. A. Collins, J. D. Kress, S. R. Bickham, T. J. Lenosky, and N. J. Troullier, *High Pressure Research* **16**, 313 (2000).
 - ¹² A. E. Mattsson, P. A. Schultz, M. P. Desjarlais, T. R. Mattsson, and K. Leung, *Model. Simul. Mater. Sci. Eng.* **13**, R1 (2005).
 - ¹³ W. J. Nellis, A. C. Mitchell, P. C. McCandless, D. J. Erskine, and S. T. Weir, *Phys. Rev. Lett.* **68**, 2937 (1992).
 - ¹⁴ S. T. Weir, A. C. Mitchell, and W. J. Nellis, *Phys. Rev. Lett.* **76**, 1860 (1996).
 - ¹⁵ W. J. Nellis, S. T. Weir, and A. C. Mitchell, *Phys. Rev. B* **59**, 3434 (1999).
 - ¹⁶ R. Redmer, *High Pressure Research* **16**, 345 (2000).
 - ¹⁷ R. Redmer, G. Röpke, S. Kuhlbrodt, and H. Reinholz, *Phys. Rev. B* **63**, 233104 (2001).
 - ¹⁸ L. A. Collins, I. Kwon, J. D. Kress, N. J. Troullier, and D. Lynch, *Phys. Rev. E* **52**, 6202 (1995).
 - ¹⁹ T. J. Lenosky, J. D. Kress, L. A. Collins, and I. Kwon, *Phys. Rev. B* **55**, 11907 (1997).
 - ²⁰ L. A. Collins, S. R. Bickham, J. D. Kress, S. Mazevet, T. J. Lenosky, N. J. Troullier, and W. Windl, *Phys. Rev. B* **63**, 184110 (2001).
 - ²¹ M. P. Desjarlais, J. D. Kress, , and L. A. Collins, *Phys. Rev. E* **66**, 025401 (2002).
 - ²² M. P. Desjarlais, *Phys. Rev. B* **68**, 064204 (2003).

- ²³ D. Klakow, C. Toepffer, and P.-G. Reinhard, *J. Chem. Phys.* **101**, 10766 (1994).
- ²⁴ S. Nagel, R. Redmer, G. Röpke, M. Knaup, and C. Toepffer, *Phys. Rev. E* **57**, 5572 (1998).
- ²⁵ M. Knaup, P.-G. Reinhard, and C. Toepffer, *Contrib. Plasma Phys.* **39**, 57 (1999).
- ²⁶ M. Knaup, G. Zwicknagel, P.-G. Reinhard, and C. Toepffer, *Nucl. Instr. Meth. A* **464**, 267 (2001).
- ²⁷ M. Knaup, P.-G. Reinhard, C. Toepffer, and G. Zwicknagel, *J. Phys. A: Math. Gen.* **36**, 6165 (2003).
- ²⁸ B. Jakob, P.-G. Reinhard, C. Toepffer, and G. Zwicknagel, *Phys. Rev. E* **76**, 036406 (2007).
- ²⁹ P. Hohenberg and W. Kohn, *Phys. Rev.* **136**, B864 (1964).
- ³⁰ W. Kohn and L. J. Sham, *Phys. Rev.* **140**, A1133 (1965).
- ³¹ N. D. Mermin, *Phys. Rev.* **137**, A1441 (1965).
- ³² G. Kresse and J. Hafner, *Phys. Rev. B* **47**, 558 (1993).
- ³³ G. Kresse and J. Hafner, *Phys. Rev. B* **49**, 14251 (1994).
- ³⁴ G. Kresse and J. Hafner, *Phys. Rev. B* **54**, 11169 (1996).
- ³⁵ G. Kresse and D. Joubert, *Phys. Rev. B* **59**, 1758 (1999).
- ³⁶ J. P. Perdew, K. Burke, and M. Ernzerhof, *Phys. Rev. Lett.* **77**, 3865 (1999).
- ³⁷ S. Nosé, *J. Chem. Phys.* **81**, 511 (1983).
- ³⁸ A. Baldereschi, *Phys. Rev. B* **7**, 5212 (1973).
- ³⁹ A. Kietzmann, B. Holst, R. Redmer, M. P. Desjarlais, and T. R. Mattsson, *Phys. Rev. Lett.* **98**, 190602 (2007).
- ⁴⁰ J. Vorberger, I. Tamblyn, B. Militzer, and S. A. Bonev, *Phys. Rev. B* **75**, 024206 (2007).
- ⁴¹ D. Beule, W. Ebeling, A. Förster, H. Juranek, R. Redmer, and G. Röpke, *Phys. Rev. E* **63**, 060202 (2001).
- ⁴² H. Juranek and R. Redmer, *J. Chem. Phys.* **112**, 3780 (2000).
- ⁴³ H. Juranek, R. Redmer, and Y. Rosenfeld, *J. Chem. Phys.* **117**, 1768 (2002).
- ⁴⁴ B. Holst, N. Nettelmann, and R. Redmer, *Contrib. Plasma Phys.* **47**, 368 (2007).
- ⁴⁵ D. Saumon, G. Chabrier, and H. M. van Horn, *Astrophys. J. Suppl. Ser.* **99**, 713 (1995).
- ⁴⁶ T. J. Lenosky, J. D. Kress, and L. A. Collins, *Phys. Rev. B* **56**, 5164 (1997).
- ⁴⁷ D. Beule, W. Ebeling, A. Förster, H. Juranek, S. Nagel, R. Redmer, and G. Röpke, *Phys. Rev. B* **59**, 14177 (1999).
- ⁴⁸ W. J. Nellis, A. C. Mitchell, M. van Thiel, G. J. Devine, R. J. Trainor, and N. Brown, *J. Chem. Phys.* **79**, 1480 (1983).
- ⁴⁹ G. V. Boriskov, A. I. Bykov, R. I. Il'Kaev, V. D. Selemir, G. V. Simakov, R. F. Trunin, V. D. Urlin, A. N. Shuikin, and W. J. Nellis, *Phys. Rev. B* **71**, 092104 (2005).
- ⁵⁰ T. J. Lenosky, S. R. Bickham, J. D. Kress, and L. A. Collins, *Phys. Rev. B* **61**, 1 (2000).
- ⁵¹ B. Militzer, D. M. Ceperley, J. D. Kress, J. D. Johnson, L. A. Collins, and S. Mazevet, *Phys. Rev. Lett.* **87**, 275502 (2002).
- ⁵² M. Ross, *Phys. Rev. B* **68**, 669 (1998).
- ⁵³ G. I. Kerley, *Tech. Rep. SAND2003-3613*, Sandia National Laboratories (2003).
- ⁵⁴ B. Militzer and D. M. Ceperley, *Phys. Rev. Lett.* **85**, 1890 (2000).
- ⁵⁵ R. Kubo, *J. Phys. Soc. Jpn.* **12**, 570 (1957).
- ⁵⁶ D. A. Greenwood, *Proc. Phys. Soc. London* **71**, 585 (1958).
- ⁵⁷ H. J. Monkhorst and J. D. Pack, *Phys. Rev. B* **13**, 5188 (1976).
- ⁵⁸ P. M. Celliers, G. W. Collins, L. B. DaSilva, D. M. Gold, R. Cauble, R. J. Wallace, M. E. Foord, and B. A. Hammel, *Phys. Rev. Lett.* **84**, 5564 (2000).
- ⁵⁹ R. Redmer, H. Juranek, N. Nettelmann, and B. Holst, in *AIP Conf. Proc. 845: Shock Compression of Condensed Matter - 2005*, edited by M. D. Furnish, M. Elert, T. P. Russell, and C. T. White (AIP, Melville, New York, 2006), pp. 127–130.
- ⁶⁰ S. Kuhlbrodt, B. Holst, and R. Redmer, *Contrib. Plasma Phys.* **45**, 73 (2005), the COMPTRA04 source code and data files can be found at <http://www.physik.uni-rostock.de/statphys/pages/compra>.